Magnetomorphic Oscillations in the Electrical Conductivity of Cadmium Cylinders

H. J. MACKEY, J. R. SYBERT, AND R. D. HIGHT
Department of Physics, North Texas State Univerxity, Denton, Texas 76203
(Received 21 August 1969)

Magnetomorphic oscillations have been observed in the Hall resistivity and magnetoresistivity of cylindrical samples of 99.9999%-grade cadmium. The magnetic field was directed along [0001], normal to the cylinder axis. The oscillations are due to the lens-shaped pocket of electrons in the third zone. No evidence of harmonics or of a contribution of the "hole arms" of the second zone was observed. The data are compared with theoretical expressions for period, phase, and dependence of amplitude on magnetic field. The period is shown to be proportional to the ratio g/d, where g is the Gaussian radius of curvature of the lens apex and d is the cylinder diameter. The amplitude is shown to damp more rapidly with magnetic field as the diameter is decreased, approaching the theoretical rate $H^{\frac{1}{2}-}$ for larger samples. Values computed for the relative phase are in disagreement with theory.

INTRODUCTION

WHEN studying transport effects in highly-pure metals at low temperatures, where the electronic mean free path λ may be on the order of millimeters, electron scattering at the boundaries of small samples may cause significant deviations from bulk phenomena observed in samples whose dimensions are large compared to λ. One of the most interesting cases is that of a thin slab of thickness a in a magnetic field directed along the sample normal and parallel to the thin dimension. Sondheimer[1] predicted theoretically that the elements of the isothermal conductivity tensor $\hat{\sigma}$ should have components which are oscillatory in the magnetic field. His results for these components $\tilde{\sigma}_{ij}$ may be written[2] as

$$\tilde{\sigma}_{11}=3nec(H_0^3/H^4)e^{-a/\lambda}\cos(2\pi H/P_0)\,, \tag{1a}$$

$$\tilde{\sigma}_{12}=3nec(H_0^3/H^4)e^{-a/\lambda}\cos(2\pi H/P_0+\tfrac{1}{2}\pi)\,, \tag{1b}$$

$$P_0=2\pi H_0=2\pi p_F c/ea\,. \tag{1c}$$

The above results were obtained under the assumptions of a spherical Fermi surface, an isotropic relaxation time, and diffuse scattering at the sample boundaries. Equation (1c) shows that the period is a direct measure of the Fermi radius p_F. This theory has been extended by Grenier *et al.*[2] to the case of Fermi surfaces of revolution about the sample normal, and has been further extended by Gurevich[3] to the case of essentially arbitrary Fermi surfaces with magnetic field tilted with respect to the sample normal. Gurevich finds the period to be given by

$$P_0=gc\cos\theta/ea\,, \tag{2}$$

where θ is the tilt angle and g is the Gaussian radius of curvature of the Fermi surface at the elliptic point where the electronic velocity is parallel to the magnetic field. Equation (2) has been verified by a different theoretical approach[4] for the case of ellipsoidal Fermi surfaces. The first experimental observations[5] of size-effect oscillations were made on an 80-μ sodium wire where highly-damped oscillations were observed in the magnetoresistance. Although the specimen was cylindrical, Eq. (1c) was used employing the diameter of the wire (in place of the film thickness a) and the measured period to compute the known Fermi radius. The result was accurate to about 2%. Since that time, many observations of oscillations have been made in various metals in the Sondheimer geometry. Mackey, Deering, and Sybert[6] have extended the Sondheimer theory to the case of a cylindrical sample with magnetic field normal to the cylinder axis. The results of this theory are given as

$$\tilde{\sigma}_{11}=6(2/\pi)^{1/2}nec(H_0^{7/2}/H^{9/2})e^{-d/\lambda}\cos(2\pi H/P_0+\tfrac{1}{4}\pi)\,, \tag{3a}$$

$$\tilde{\sigma}_{12}=-6(2/\pi)^{1/2}nec(H_0^{7/2}/H^{9/2})e^{-d/\lambda}\times\cos(2\pi H/P_0-\tfrac{1}{4}\pi)\,, \tag{3b}$$

$$P_0=2\pi H_0=2\pi p_F c/ed\,, \tag{3c}$$

where d is the diameter of the cylinder. Equations (3) may be compared to Eqs. (1) to note the difference to be expected between the thin film and cylindrical sample geometries. One sees that the cylinder diameter replaces the film thickness, that the cylinder data are expected to fall off as $H^{-9/2}$ as compared to H^{-4} for the film data, and, although both theories give $\frac{1}{2}\pi$ as the phase difference between $\tilde{\sigma}_{11}$ and $\tilde{\sigma}_{12}$, the absolute phases are different. This paper reports on data measured in cylindrical samples of cadmium with magnetic field normal to the cylinder axis, parallel to [0001]. The results are discussed in terms of Eqs. (3).

[1] E. H. Sondheimer, Phys. Rev. **80**, 401 (1950).
[2] C. G. Grenier, K. R. Efferson, and J. M. Reynolds, Phys. Rev. **143**, 406 (1966).
[3] V. L. Gurevich, Zh. Eksperim. i Teor. Fiz. **35**, 668 (1958) [English transl.: Soviet Phys.—JETP **8**, 464 (1959)].
[4] H. J. Mackey, J. R. Sybert, and W. D. Deering, Phys. Rev. **175**, 729 (1968).
[5] J. Babiskin and P. H. Siebenmann, Phys. Rev. **107**, 1249 (1957).
[6] H. J. Mackey, W. D. Deering, and J. R. Sybert, Phys. Rev. **180**, 678 (1960).

EXPERIMENTAL PROCEDURE

The various single-crystal samples were prepared from an ingot of 99.9999%-grade cadmium obtained from Cominco Products, Inc., Spokane, Wash. The resistivity ratio $R_{293}/R_{4.2}=1.14\times10^4$ was measured in a cylindrical sample of diameter 1.05 mm. Samples were trepanned out of x-ray–oriented crystals (see Fig. 1) by spark erosion on a Servomet Spark Cutter, Model SMD, operated on the range-6 setting. Figure 2 shows the tool design employed. The hole through which the cylinder is trepanned is approximately 0.2 mm greater than the desired cylinder diameter. The large openings just above the short-cylinder hole allow free flushing of swarf, and this, along with the short cutting length, reduces side arcing which occurs when the cutting cylinder is made as long as the sample to be prepared. Cylinders were obtained having less than 2% taper along their length and cross sections which were circular to better than 1%. Leads of No. 34 enameled copper wire were originally soldered to the samples with Cerroseal 35 solder (50-50 In-Sn), as indicated in Fig. 9.

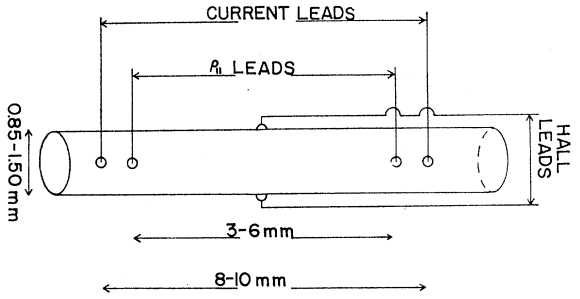

FIG. 1. Diagram indicating electrical connections to cylindrical sample. The crystal binary axis [10$\bar{1}$0] is along the cylinder axis.

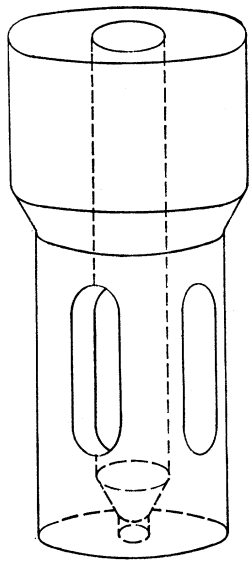

FIG. 2. Illustration of trepanning tool.

Because of complications discussed below, leads were spot welded to the samples by charging a 60-μF capacitor to 120 V and discharging it through about 3 in. of the lead wires. It was possible to make excellent connections which were firmly attached to very small points and were not at all electrically noisy. The cylinders were suspended in a Dewar with the cylindrical axis in the vertical. A fixed magnetic field was rotated in the horizontal plane about the vertical binary axis to obtain a polar plot of magnetoresistance as indicated in Fig. 3. The deep minimum at [$\bar{1}$2$\bar{1}$0] was located to within $\frac{1}{2}$°, and the magnet was then rotated 90° to align the magnetic field along [0001]. Potentials on the Hall and magnetoresistance leads were measured by recording the off-balance of a Honeywell six-dial thermal-free potentiometer, amplified by a Keithley Model 148 nanovoltmeter. The analog output of the Keithley and the output of a Bell Hall-Pak Model BH-701 which sampled the magnetic field were fed to two channels of a magnetic tape-digital recorder system. These analog data were digitized by a Model 7100A Fairchild 5-digit integrating digital voltmeter whose BCD output was recorded by a Kennedy Model 1400 incremental magnetic tape recorder. This system is capable of recording two data points per second, yielding approximately 3000 data points for a 25-min sweep of the magnetic field. The data were simultaneously recorded on a strip-chart recorder for visual inspection. These extremely dense data were processed on IBM 1400 and IBM 1620 digital computers. The

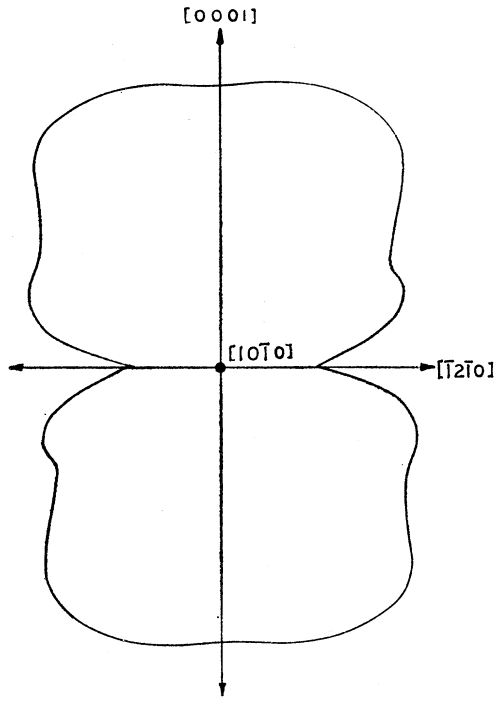

FIG. 3. Polar plot of magnetoresistance of cadmium in plane perpendicular to the binary axis (in arbitrary units).

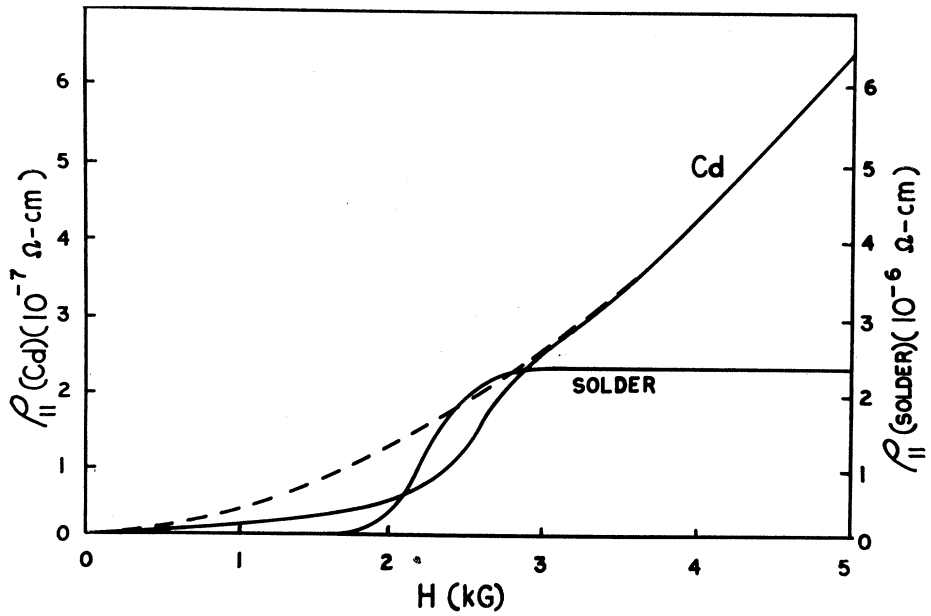

FIG. 4. Magnetoresistivities of cadmium and Cerroseal 35 solder at 1.3°K showing the effect of the superconducting transition of the solder. The dashed curve is a quadratic extrapolation of the data above the transition to the low-field region.

data were smoothed incrementally and printed out at 25-G intervals. The gross data were then curve fit by least squares to a quadratic and/or cubic polynomial, and the superimposed oscillations were obtained by subtraction.

EXPERIMENTAL RESULTS AND DISCUSSION

Initial measurements of the magnetoresistivity ρ_{11} gave results as indicated in Fig. 4. The presence of a very large hump was traced to the effect of the solder, which was used to attach the leads, going through a superconducting transition. Because of the small diameter of the cylindrical samples, the superconducting solder effectively shorted out an appreciable fraction of the length of the sample resulting in a decreased potential. Figure 4 illustrates the magnetic behavior or Cerroseal 35 solder. At 4.2°K, the solder begins to go normal at 704 G, essentially saturating to a constant resistivity at approximately 1500 G. At 1.3°K, the solder begins to go normal at 1700 G, saturating by about 2700 G. Because of this effect, leads were spot welded onto the sample, resulting in a normal quadratic magneoresistance. Figures 5 and 6 indicate the oscillatory component $\tilde{\rho}_{11}$ measured in samples of

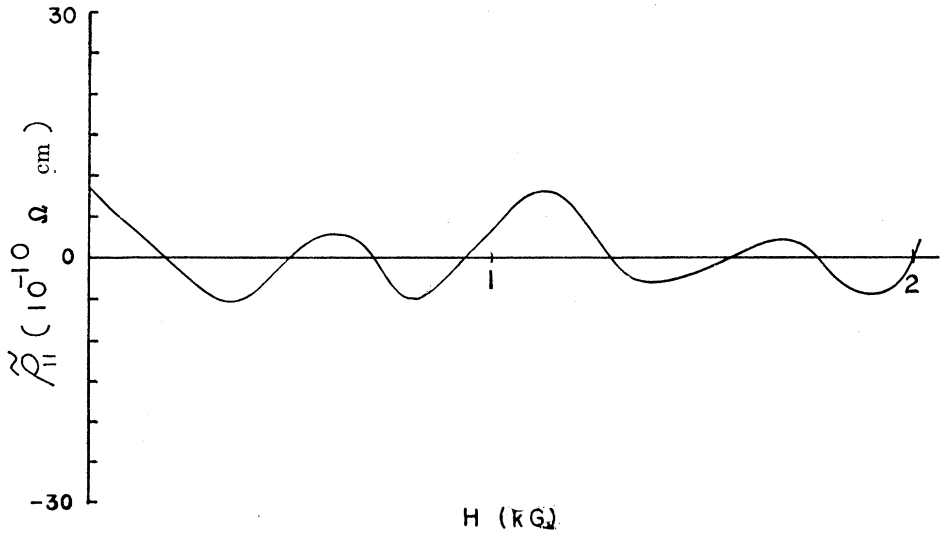

FIG. 5. The oscillatory component $\tilde{\rho}_{11}$ for the 1.05-mm sample.

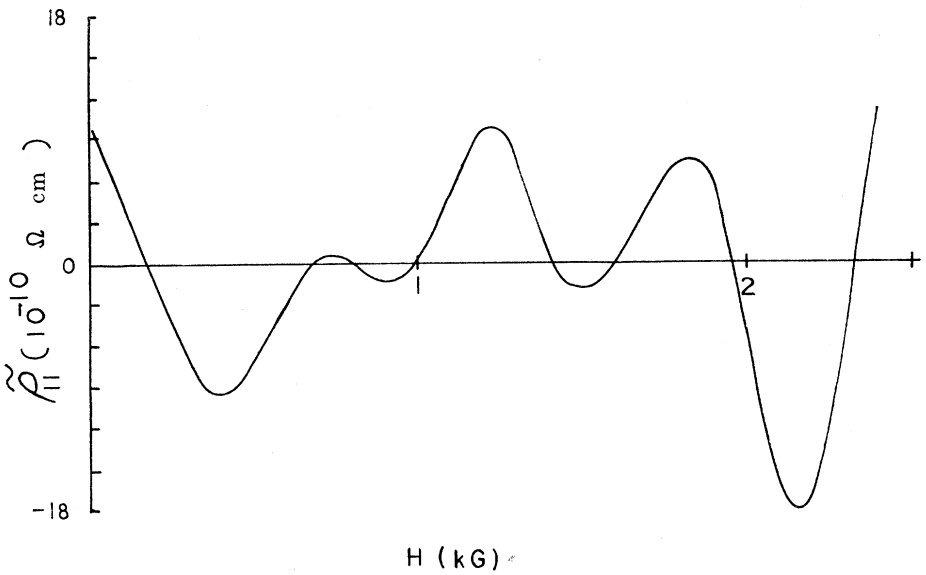

FIG. 6. The oscillatory component $\tilde{\rho}_{11}$ for the 0.90-mm sample.

diameter 1.05 and 0.90 mm, respectively. It had been hoped that sufficiently accurate data could be obtained from magnetoresistance measurements alone because of the difficulty of attaching Hall leads with solder points is small compared to the cylinder diameters. For this reason, no Hall leads were attached to these two samples. The wander in the baseline indicated in these figures is due to the fact that the ratio $\tilde{\rho}_{11}/\rho_{11}$ is on the order of 0.03 at 1 kG and decreases quadratically (or faster) as the field is increased. Thus, even with extensive data smoothing by computer it is possible to recover only marginally acceptable $\tilde{\rho}_{11}$ data from ρ_{11} data. At this point, it was decided to attach Hall leads by spot welding. This was done on two separate samples of diameters 1.26 and 0.85 mm. The resulting $\tilde{\rho}_{21}$ data are indicated in Figs. 7 and 8, respectively. These data are much cleaner than the $\tilde{\rho}_{11}$ data of Figs. 5 and 6 due to the fact that $\tilde{\rho}_{21}/\rho_{21}$ is much larger than $\tilde{\rho}_{11}/\rho_{11}$. Tensor inversion of $\hat{\rho}$ gives

$$\sigma_{11}=\rho_{11}/(\rho_{11}^2+\rho_{21}^2), \tag{4a}$$

$$\sigma_{12}=\rho_{21}/(\rho_{11}^2+\rho_{21}^2). \tag{4b}$$

Since the gross component ρ_{11g} is quadratic in magnetic field for cadmium, $\rho_{11g}\gg\tilde{\rho}_{11}$, and since $\rho_{11g}\gg\rho_{21}$, one obtains, at high field,

$$\rho_{11g}=\alpha H^2, \tag{5a}$$

$$\tilde{\rho}_{11}\simeq\rho_{11g}^2\tilde{\sigma}_{11}=\alpha^2H^4\tilde{\sigma}_{11}, \tag{5b}$$

$$\tilde{\rho}_{21}\simeq\rho_{11g}^2\tilde{\sigma}_{12}=\alpha^2H^4\tilde{\sigma}_{12}. \tag{5c}$$

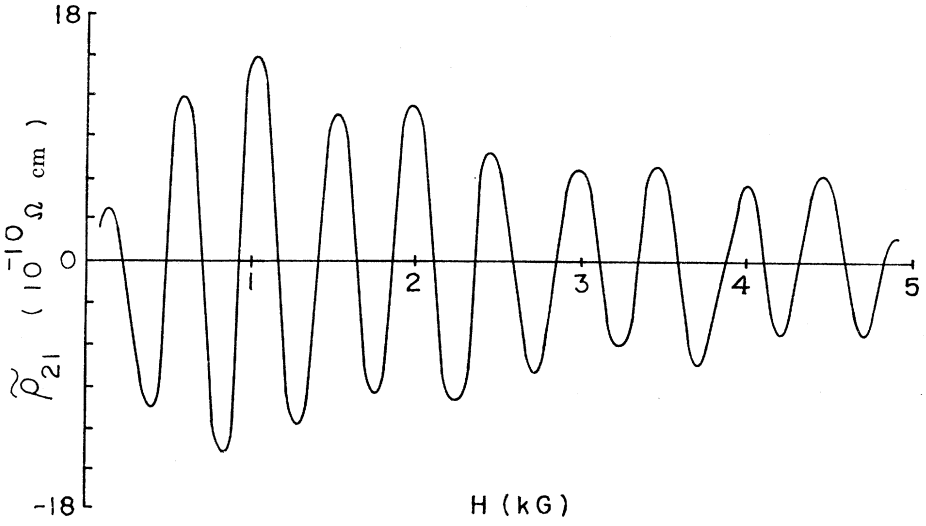

FIG. 7. The oscillatory component $\tilde{\rho}_{21}$ for the 1.26-mm sample.

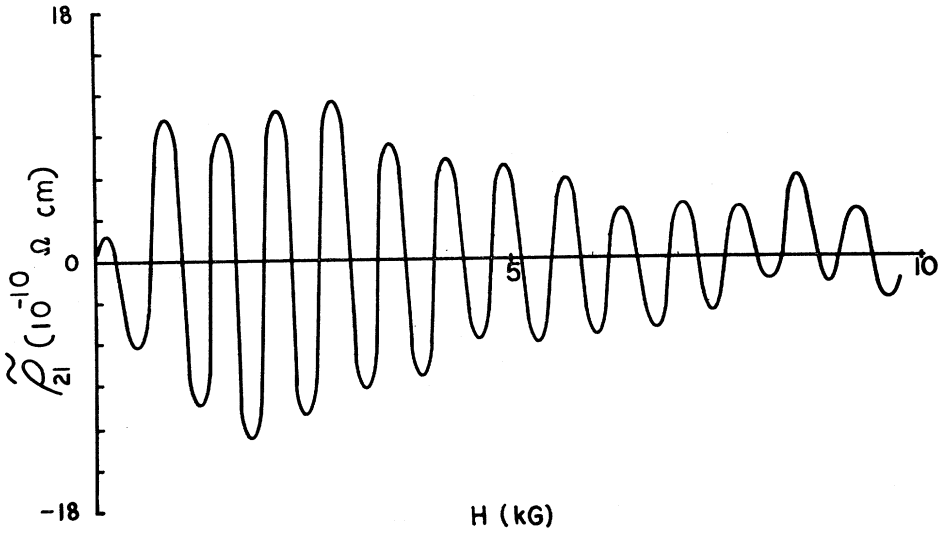

FIG. 8. The oscillatory component $\tilde{\rho}_{21}$ for the 0.85-mm sample.

Equation (3), therefore, predicts that the $\tilde{\rho}_{ij}$ should exhibit maxima at magnetic field values given by

$$H_n = P_0(n - \delta/2\pi), \tag{6}$$

where $n=0, 1, 2, \ldots$ with $\delta = -\frac{3}{4}\pi$ for $\tilde{\rho}_{11}$ and $\delta = +\frac{3}{4}\pi$ for $\tilde{\rho}_{21}$. Thus, a plot of the values of magnetic field at which extrema occur against the integers (minima positions plotted at the half-integers) should yield a straight line whose slope is the period P_0 and whose intercept is a measure of the phase δ. Figure 9 is such a plot for the four samples studied. Straight lines were fitted to the data by least squares. Table I gives a summary of the results obtained. It has been previously well established[2] that the lens-shaped pocket of electrons in the third zone is responsible for the major Sondheimer oscillations in cadmium. Grenier *et al.*[2] have also observed a contribution due to the "hole arms" in the second zone producing a period approximately 25% and an amplitude of about 10% of the electron oscillations. Although the theory for cylindrical geometry has assumed a spherical Fermi surface, one may reasonably assume that the Fermi momentum p_F which occurs in Eq. (3c) may be replaced by g, the Gaussian radius of curvature of the apex of the lens surface in accordance with the results of Gurevich. Using $g=1.45\times10^{-19}$ cgs$=0.972\ p_F$, as determined in Ref. 7, one then obtains the expression

$$d = 569/P_0 \text{ mm}, \tag{7}$$

relating the cylinder diameter d to the period P_0 of the lens oscillations when P_0 is expressed in gauss. One may insert the measured period into Eq. (7) to calculate d_{eff}, the effective diameter. Table I contains

TABLE I. Summary of numerical results.

d (mm)	$\tilde{\rho}_{ij}$	P_0 (G)	δ (deg)	d_{eff}/d
1.05	$\tilde{\rho}_{11}$	527	−45.2	1.03
0.90	$\tilde{\rho}_{11}$	583	−47.6	1.08
1.26	$\tilde{\rho}_{21}$	485	−49.6	0.93
0.85	$\tilde{\rho}_{21}$	701	−37.4	0.95

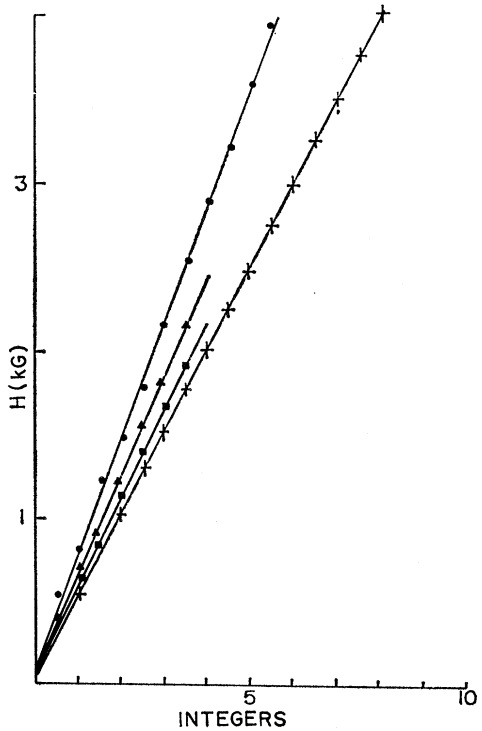

FIG. 9. Period and phase plot for the four samples. The squares triangles, crosses, and solid circles correspond to the data of Figs. 5, 6, 7, and 8, respectively.

[7] H. J. Mackey, J. R. Sybert, and J. T. Fielder, Phys. Rev. 157, 578 (1967).

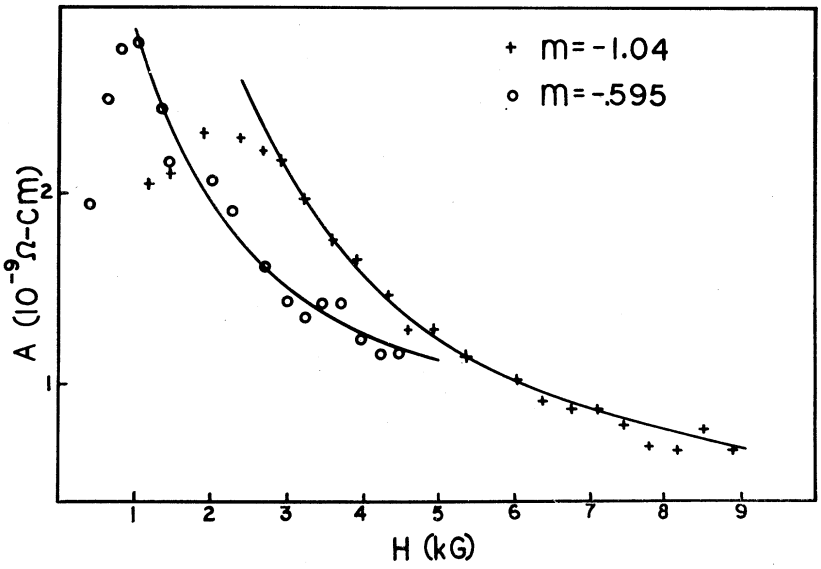

FIG. 10. Plot of the peak-to-peak amplitudes observed in $\tilde{\rho}_{21}$ for the 1.26-mm (circles) and 0.85-mm (crosses) samples versus magnetic field. Least-squares curves of the form $y=aH^m$ are indicated.

the entry d_{eff}/d, where d is the measured diameter. This quantity should equal one for exact agreement with theory. It is seen that the error ranges from -7 to $+8\%$. It is most probable that the period is actually determined by the ratio g/d, and that the noted error is purely experimental. It should be pointed out, however, that the oscillatory expressions given in Eqs. (3) are obtained as asymptotic functions valid at high field. Thus, inclusion of all maxima and minima in the plots of Fig. 9 is not strictly correct. Equations (3) imply that $\delta=-135°$ for $\tilde{\rho}_{11}$ and $+135°$ for $\tilde{\rho}_{21}$. As seen in Table I, δ appears to be approximately $-45°$ for both $\tilde{\rho}_{11}$ and $\tilde{\rho}_{21}$. As noted above, the $\tilde{\rho}_{11}$ data are marginal, and the question of relative phase is not determined. Equations (3) imply that $\tilde{\rho}_{11}$ and $\tilde{\rho}_{21}$ should damp as $H^{-1/2}$. Figure 10 is a plot of the peak-to-peak amplitudes observed in the two $\tilde{\rho}_{21}$ samples. The amplitude grows at first and then decreases. Ignoring the initial rise, a logarithmic least-squares fit was made to $y=ax^m$ to estimate the damping exponent m. The exponent was found to be $m=-1.04$ for the 0.85 mm sample, and $m=-0.595$ for the 1.26 mm sample. Although the spark-cut samples were treated with a light HNO_3 polish, there probably remains a shallow distorted region at the sample surface. This is consistent with the $(d_{\text{eff}}/d)<1$ values found for the clean $\tilde{\rho}_{21}$ data. Such a distortion layer would increase the damping rate and would be more significant percent wise in smaller samples. Thus, although not demonstrated to be 0.5, it is likely that the true absolute value of m is less than 0.6. Figure 11 shows the results of a computer calculation[8] of the power density spectrum for the $\tilde{\rho}_{21}$ data of Fig. 8. Although this technique does not give accurate period determinations for this limited number of periods, it is quite sensitive in that noticeable peaks are produced for very low-amplitude sinusoid content.

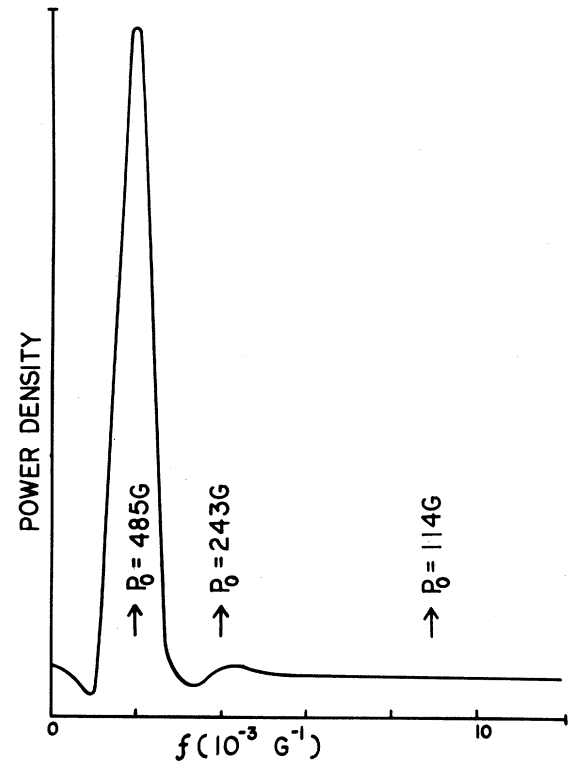

FIG. 11. Plot of power density (arbitrary units) as a function of frequency for the $\tilde{\rho}_{21}$ data of Fig. 8. Arrows indicate the positions to be expected for peaks due to the fundamental electron oscillation, its second harmonic, and the hole oscillations.

[8] J. S. Bendat and A. G. Piersol, *Measurement and Analysis of Random Data* (John Wiley & Sons, Inc., New York, 1966), pp. 291ff.

The plot clearly indicates no evidence for the presence of harmonics of the lens oscillations or for the presence of the short-period Grenier oscillations.

It has been demonstrated that submillimeter diameter cylinders may be prepared by spark-trepanning without significant reduction in the bulk mean free path. This is evidenced by the fact that the observed oscillations are of approximately the same amplitude as those observed in Sondheimer samples of equivalent thickness. The use of cylindrical samples in conjunction with field-modulation detection of the oscillations will allow probing of the curvature of Fermi surfaces by rotation of the magnetic field without the complication of loss of sample symmetry. Further, the order of magnitude increase in practical current density results in an equivalent increase in signal.

PHYSICAL REVIEW B VOLUME 1, NUMBER 6 15 MARCH 1970

Scattering-Center Effects in the Magnetoresistance of Nickel

F. C. SCHWERER

Department of Applied Physics, Cornell University, Ithaca, New York 14850 and Edgar C. Bain Laboratory for Fundamental Research, U. S. Steel Corporation Research Laboratory, Monroeville, Pennsylvania 15146*

AND

J. SILCOX

Department of Applied Physics, Cornell University, Ithaca, New York 14850

(Received 11 September 1969)

The magnetoresistance of many polycrystalline samples of nickel alloyed with small concentrations of iron, cobalt, manganese, chromium, and carbon has been measured. An analysis of the data gave the result that all those specimens in which the conduction-electron scattering was dominated by one particular scattering center were found to obey Kohler's rule. However, the details of the magnetoresistance were different in each case, with the exception of the iron, cobalt, and manganese impurities, which formed one group. In addition, the thermal-scattering magnetoresistance and that due to deformation were different again. These observations confirm previous conclusions concerning the validity of Kohler's rule. Extremely large magnetoresistance was found for the iron, cobalt, and manganese group of impurities as scattering centers, which apparently is much larger than observed in any other system. This can be correlated with other electronic properties of the impurities, such as the resistivity and magnetic moment per unit concentration. In particular, the high magnetoresistance appears associated with the presence of large local moments. The zero-field anisotropy in the resistance is also correlated with these same properties. In spite of this correlation, we have no clear interpretation of the extreme magnetoresistance.

I. INTRODUCTION

NOW that properties of the Fermi surface have become relatively well understood, the role of electron scattering processes has become of importance in understanding some of the electronic transport properties of metals. We note recent work by Dugdale and Basinski[1] relating breakdowns in Matthiessen's rule in noble metals to anisotropies in the relaxation times and work by Bailyn and Dugdale[2] on effects in the electronic contribution to the thermoelectric power, again in the noble-metal alloys. Attention to this aspect of transport properties was first drawn by Coles[3] in connection with Hall effect studies. Since then, further work has been contributed by Cooper and Raimes,[4] Ziman,[5] Hurd,[6] and Heine.[7] In particular, Ziman has given a discussion of transport properties in noble-metal alloy systems based on well-known Fermi-surface properties and shown that in some cases considerable anisotropy in the relaxation times could be concluded from the experimental results. Deaton and Gavenda[8] have made direct measurements of these anisotropies in copper. Most of the work to data has been carried out on noble-metal alloys. In this paper, we are concerned with magnetoresistance measurements on very dilute alloys of nickel in which effects thought to be due to electron scattering effects are identified. Rather large breakdowns in Matthiessen's rule in more concentrated alloys of the same type have recently been identified by Fert and Campbell[9] and by Farrell and Greig[10] and identified by them as due to spin mixing (see Campbell, Fert and Pomeroy,[11] and Bourquard, Daniel and Fert[12]).

* Present address.

[1] J. S. Dugdale and Z. S. Basinski, Phys. Rev. **157**, 552 (1967).

[2] M. Bailyn, Phys. Rev. **157**, 480 (1967); J. S. Dugdale and M. Bailyn, *ibid.* **157**, 485 (1967).

[3] B. R. Coles, Phys. Rev. **101**, 1254 (1956).

[4] J. R. A. Cooper and S. Raimes, Phil. Mag. **4**, 145 (1959).

[5] J. M. Ziman, Phys. Rev. **121**, 1320 (1961).

[6] C. M. Hurd, Phil. Mag. **12**, 47 (1965).

[7] V. Heine, Phil. Mag. **12**, 53 (1965).

[8] B. C. Deaton and J. D. Gavenda, Phys. Rev. **129**, 1990 (1963).

[9] A. Fert and I. A. Campbell, Phys. Rev. Letters **21**, 1190 (1968).

[10] T. Farrell and D. Greig, J. Phys. **C1**, 1359 (1968).

[11] I. A. Campbell, A. Fert, and A. R. Pomeroy, Phil. Mag. **15**, 977 (1967).

[12] A. Bourquard, E. Daniel, and A. Fert, Phys. Letters **26A**, 260 (1968).